11th AIAA/CEAS Aeroacoustics Conference (26th AIAA Aeroacoustics Conference)
23 - 25 May 2005, Monterey, California

AIAA 2005-2855

Measurements of the wavenumber-frequency spectrum of wall pressure fluctuations under turbulent flows

B.Arguillat[*] and D. Ricot[†]

Renault, Guyancourt, France

G.Robert[‡] and C.Bailly[§]

LMFA, UMR CNRS 5509 & Ecole Centrale de Lyon, Ecully, France

    The prediction of the vibratory response of structures excited by turbulent flows implies a good knowledge of both aerodynamic and acoustic components of the wall pressure fluctuations. In the present work, experiments were aimed at measuring wall pressure fluctuations under turbulent flows, in order to separate the two exciting loadings. The experiments were conducted in the anechoic wind tunnel of Ecole Centrale de Lyon (France). Two configurations were more precisely studied : a turbulent boundary layer and a cylindrical bar in crossflow. A rotative array has been designed that allows the measurement of a complete map of cross-power spectral densities over a large area. A post-processing has been developed to transform the space-frequency data into wavenumber-frequency spectra. Results for the boundary layer are consistent with the Corcos model. Analysis of the spectra shows the presence of an acoustic pressure field, which magnitude is about 5% of the aerodynamic pressure field. Concerning the bar, the whistling frequencies do appear on wavenumber spectra, but not the broadband acoustic field previously observed for the boundary layer. Besides, the strong flow inhomogeneity makes quality of wavenumber spectra worse.

Nomenclature

k_c aerodynamic wavenumber
k_0 acoustic wavenumber
S_{ij} cross-power spectral density between points i and j, Pa^2/Hz
Φ wavenumber-frequency power spectral density, Pa^{2}m^{2}s/rad^3
APS   Auto-Power Spectral density
CPS   Cross-Power Spectral density

I. Introduction

A. Automotive context

The notion of comfort in the cockpit of a car depends on many parameters, one of them being the noise experienced by the driver and his passengers. The use of high quality audio and vocal recognition systems makes it essential to reduce noise inside cars. Since engine, exhaust and tyre noise have been of particular attention these last ten years, and have been then considerably improved, car manufacturers are becoming more and more concerned about the reduction of wind noise in their production vehicles.

  [*]Ph. D. student, blandine.arguillat@renault.com, Renault, Research Division, 1 avenue du Golf, TCR AVA 1 63, 78288 Guyancourt Cedex France.

  [†]Doctor, denis.ricot@renault.com, Renault, Research Division, 1 avenue du Golf, TCR AVA 1 63, 78288 Guyancourt Cedex France.

  [‡]Assistant Professor, gilles.robert@ec-lyon.fr, LMFA, 36 avenue Guy de Collongue, 69134 Ecully Cedex France.

  [§]Professor, Senior Member AIAA, christophe.bailly@ec-lyon.fr, LMFA, 36 avenue Guy de Collongue, 69134 Ecully Cedex France.

American Institute of Aeronautics and Astronautics

Aerodynamic noise is perceptible from 100 km/h on and is dominant at about 130 km/h. This noise is emitted over a broad frequency range, making it difficult to control.[1] The principal sources of broadband noise are the phenomena of separation and reattachement of the airflow around the car body. Above them, the flow pattern of the A-pillar vortex is of particular interest for two reasons : first because of its proximity with the ears of passengers, and second because it is very energetic. The aeroacoustic prediction faces the problem of flow-induced structural loading to be coupled with the panel, in this case the front side window. Bremner and Wilby[2] showed that both aerodynamic pressure and acoustic pressure loading have to be taken into account for the prediction of structural response of the window. Acoustic pressure is however very small compared to turbulent pressure (about 2 or 3 orders of magnitude smaller in the simulation of DeJong et al.[3]), which makes it extremly difficult to measure experimentally.

One way to separate acoustic and aerodynamic pressure in the wall pressure fluctuations signal is to represent them in the wavenumber domain. Indeed, in the automotive case, the acoustic and turbulent wavenumbers are different from a factor 10, since the Mach number of interest for aerodynamic noise are about 0.1. The objective of this work is to finalize a wavenumber post-processing to separate acoustical and aerodynamic excitations on the two academic cases of a turbulent boundary layer and a cylinder in a flow.

B.   Background

Bull[4] wrote recently a review of the different wavenumber spectra measurement methods. A first approach consists of a direct measurement of the wavenumber spectral density, by spatial discrete Fourier transform of the cross-power spectral densities. This requires a low-pass wavenumber filtering and a great number of sensors according to Shannon's sampling theorem. That is why very few and only recent publications using this method are available (Ibars[5] in 1990, Manoha[6] in 1993, or Abraham[7] in 1998).

A second approach is based on the analysis of the vibratory response of a structure excited by the flow-induced pressure fluctuations. Each vibration mode filters at its own frequency the wavenumbers associated to its first modal shape. For example, Martin & Leehay or Martini cited by Blake,[8] or Robert[9] used small rectangular vibrating plates, whose responses are known. The inconvenient of this technique lies in the fact that only a few wavenumbers are accessible by this measurement.

A third way is to use arrays of pressure transducers. Maidanik[10] describes the wavevector filtering action of transducers arrays. Maidanik & Jorgensen[11] propose also enhancements to such arrays. The principle consists in obtaining, through linear combinations of signals, a wavenumber spectrum for discrete values of the wavenumber, depending on the spacing between transducers. Many authors[12,13,5,6] put this method into practice. Using the Corcos' hypothesis[14] that longitudinal and transversal fluctuations are independant, they only measured one-dimensional spectra in both directions.

The objective of this study is not limited to boundary layer flows, but extends to more complex flows for which it is not always easy to determine global longitudinal and transversal directions. That is why we choose to measure two-dimensional wavenumber spectra, which requires to measure pressure fluctuations over a surface and not only along a line.

Few studies, however, were conducted in two dimensions. One can mention the work of Sherman,[15] who evaluated the wavenumber spectrum of a water boundary layer with a 11×11 transducers square array.

II.   Experimental installation

A.   Remote microphone probes

The considered application requires a high spatial resolution, a small background noise and a large frequency range. However traditional pressure transducers used in aerodynamic measurements present a high background noise, and the acoustic transducers are of too high sensitivity (piezoelectric transducers or condenser microphones of diameter 1" or 1/2"). In term of sensisity, 1/4" and 1/8" could have been suitable, but the first ones are too big-sized and the others are too expensive.

The problem with non point sensors is that they induce a spatial averaging over their sensitive surface. This effect, initially studied by Corcos,[14] has then been reformulated by Lueptow[16] to take different types of transducers into account. One possible solution to reduce the size of the sensitive surface is to use pinhole microphones. Broadly used, for example by Callister,[17] Farabee & Casarella,[18,19] Brungart et al,[20] this system does not yet permit to bring the transducers closer from each other.

The choice has thus been made to use remote microphone probes. The interest of such a setting is twofold:

American Institute of Aeronautics and Astronautics

on the one hand the active measurement surface is reduced to the size of the tube at the wall, and on the other hand the viscous dissipation effects in the tube attenuate the level of pressure fluctuations. A classical acoustical microphone of high sensitivity can then be used. In the present work, the probes are composed of a 1/4" Brüel & Kjær microphone, placed prependicularly to a steel tube of variable diameter and of length 14 to 15 cm. At one extremity, the tube comes out on the measurement wall. At the other extremity, each metallic tube is linked to a 2 m long, 2 mm diameter choked vinyle tube. In this way, reflexions inside the tubes can be avoided.

Three different kinds of probes have been designed:

- for the big diameter probes, the metallic tube diameter is 5 mm and an adapter is used to join the vinyle tube,

- for the medium diameter probes, the section is constant (2 mm diameter),

- for the small diameter probes, the section of the tube decreases progressively to reach a diameter of 0.7 mm at the wall.

Since a large hole on the wall could have induced disturbing whistling and non-negligible flow rate fluctuations, the tubes of big and medium diameter probes do not come out directly on the wall, but through little holes of diameter 0.5 mm (9 holes for big diameter probes, 3 holes for the medium ones), as shown in Figure 1.

For geometrical reasons, the response of such probes presents oscillations due to resonances inside the metallic tube. A calibration has thus been performed in order to correct the probe responses by their own transfer function, and then recover the wall pressure.

B.   Array

The measurement array is created by placing $N = 63$ remote microphone probes along the diameter of a disk. Figure 1 shows the repartition of the transducers on the disk. On each side of the central transducer, 19 small-diameter probes are placed, with a spacing of $\Delta r_1 = 2$ mm between the center of two adjacent transducers. On both sides of small probes, there are 2×9 probes of diameter 2 mm, spaced by $\Delta r_2 = 4$ mm. Lastly, 2×3 probes of 5 mm diameter are placed on both sides of medium-diameter probes, and are spaced by $\Delta r_3 = 8$ mm.
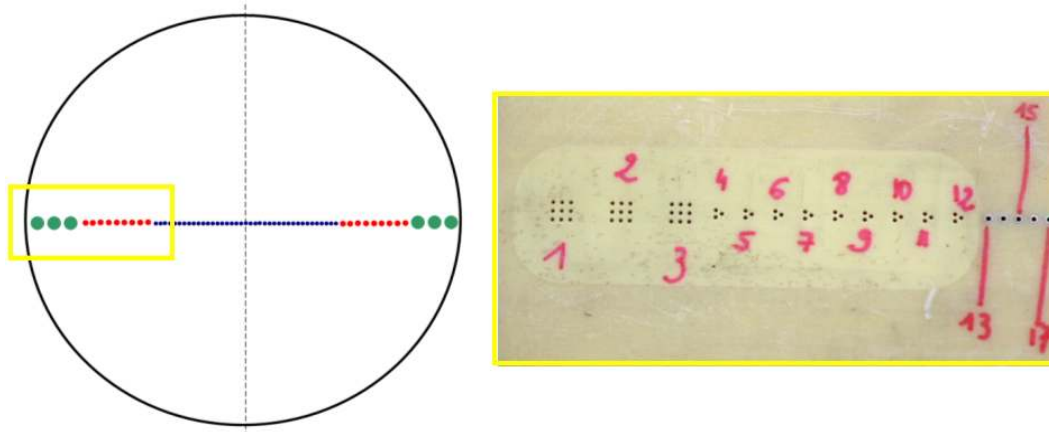

Figure 1.   *Sketch of the rotative measurement array and detail of the holes on the wall*

The measurement consists of the simultaneous recording of the pressure field measured by the probes during the time $T = 120$ s. After observing the N pressure signals during T, the transducers line is turned by an angle of $\Delta\theta = 2.9°$ around the center and a new recording of the N signals during T is done. This operation (rotation of the transducers and recording) is repeated $M = 63$ times. This allows to scan with discrete values a complete disk. So as to optimize the measurement duration, the rotation system has been motorized and operated by remote control outside the wind tunnel.

American Institute of Aeronautics and Astronautics

Figure 2 shows the auto-power spectral densities of wall pressure fluctuations measured by the three kinds of probes under a turbulent boundary layer at 40 m/s. Three beams of curves can be identified, each corresponding to a different kind of probe. As predicted by the theory,[14, 16] the biggest transducers have the lowest cut-off frequency (around 1 500 Hz). The next beam represents the medium-sized probes, whose cut-off frequency is about 3 000 Hz. And the small-diameter probes beam does not show any slope changing, which means that their cut-off frequency is above 10 000 Hz. Big and medium probes serve as low-pass wavenumber filters to eliminate large wavelengths and plug a role of anti-aliasing filter. What should also be noted in this figure is that, except at high frequencies, the probes response has been calibrated well enough to eliminate the own probe oscillatory response such that level differences among the same kind of probes remain in an acceptable range of 2 dB. By precaution, data above 6 000 Hz, which have demonstrated to present calibration defaults, will not be used.
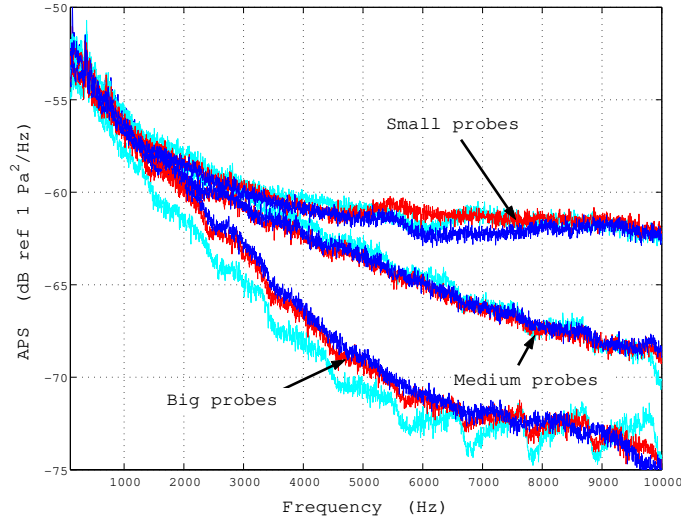

Figure 2. *Auto-power spectral densities of wall pressure fluctuations measured by the three kinds of probes under a boundary layer*

C. Post-processing

The post-processing described in this paper is the two-dimensionnal transformation of the spatial data into wavenumber spectra.

1. Definitions

Let $u(\vec{r}, t)$ be a random stationary and ergodic signals depending on space and time. We define the Fourier transform in time domain by

$$U(\vec{r}, \omega) = \frac{1}{2\pi} \int_{-\infty}^{+\infty} u(\vec{r}, t) e^{-i\omega t} dt. \tag{1}$$

The cross-power spectral density (CPS) may be defined from the signals temporal Fourier transforms (known as Wiener-Khinchin relation):

$$S_{ij}(\vec{x_i}, \vec{r}, \omega) = \lim_{\tau \to \infty} \frac{2\pi}{\tau} E[U(\vec{x_i}, \omega, \tau) U^*(\vec{x_j} = \vec{x_i} + \vec{r}, \omega, \tau)], \tag{2}$$

E standing for the expected value. The cross-spectra were calculated using a Hanning windowing on time data, a sampling frequency of 25.6 kHz, and with 400 data blocks.

As in the temporal domain, a 2D Fourier transform can be defined in the space domain by

$$U(\vec{k}, t) = \frac{1}{(2\pi)^2} \int_{-\infty}^{+\infty} \int_{-\infty}^{+\infty} u(\vec{x}, t) e^{-i\vec{k} \cdot \vec{x}} \, d\vec{x}. \tag{3}$$

American Institute of Aeronautics and Astronautics

For homogeneous fields, the cross-power spectrum do not depend on the observer point. The cross-power spectral density as a function of frequency and wavenumber, commonly called wavenumber-frequency spectrum, is then defined as the spatial Fourier transform of the CPS:

$$\Phi_u(\vec{k}, \omega) = \frac{1}{(2\pi)^2} \int_{-\infty}^{+\infty} \int_{-\infty}^{+\infty} S_{ij}(\vec{r}, \omega) e^{-i\vec{k}\cdot\vec{r}} d\vec{r}. \tag{4}$$

Note that the inverse transform, calculated at $\vec{r} = \vec{0}$, yields

$$\int_{-\infty}^{+\infty} \int_{-\infty}^{+\infty} \Phi_u(\vec{k}, \omega) d\vec{k} = S_{uu}(\vec{r} = \vec{0}, \omega). \tag{5}$$

Equation 5 is usually refered to as the Parseval equality.[21]

Practically, it is impossible to obtain the pressure field over an infinite surface and the integration is restricted to the spatial measurement domain. Moreover, measurements only give the cross-spectral densities at a finite number of discrete points, and the rotating disk implies the use of polar coordinates $\vec{x_i} = (r_n, \theta_m) = (n\Delta r, m\Delta\theta)$. The practical calculation will thus be computed from a sum and not an integral:

$$\Phi(\vec{k}, \omega) = \frac{1}{(2\pi)^2} \sum_{m=1}^{m=M} \sum_{n=1}^{n=N} S_{nm}(r_n, \theta_m, \omega) e^{-i[r_n \cos\theta_m \, k_x + r_n \sin\theta_m \, k_y]} \, r_n \, \Delta r \, \Delta\theta. \tag{6}$$

In this expression, we choose to keep the basic rectangular windowing on the spatial data, although the signal is short. Preliminary calculations demonstrated indeed that other windows, like the Hanning one, made the spectral resolution worse.

Theoretically, if the flow is homogeneous, $\Phi(\vec{k}, \omega)$ should be real. In what follows, figures show only the real part of the wavenumber transform. The spectral step is $\Delta k = 15.7$ rad/m for analytic cases and $\Delta k = 6$ rad/m for measured data. Units of figures showing Φ, if not written, are $\text{Pa}^2\text{m}^2\text{s}/\text{rad}^3$.

In order to validate the implementation of the post-processing, it was applied to analytic cases. We present here the case of a diffuse sound field, and the case of the Corcos turbulent boundary layer model.

2. Diffuse sound field

A diffuse sound field is an environment in which the pressure level is the same at any point and the acoustic energy flow is equiprobable in any direction. The cross-power spectrum between two points in spherical coordinates is given by (see Pierce[22])

$$S_{p_i p_j}(r, \theta, \omega) = S_{pp}(\omega) \frac{\sin(k_0 r)}{k_0 r}. \tag{7}$$

To obtain the wavenumber spectrum on a wall, this expression has to be integrated, using the first Bessel's integral, yielding

$$\Phi(\vec{k}, \omega) = \begin{cases} \dfrac{S_{pp}(\omega)}{2\pi k_0{}^2} \cdot \dfrac{1}{\sqrt{1 - \left(\dfrac{|\vec{k}|}{k_0}\right)^2}} & \text{if } |\vec{k}| < k_0 \\[4mm] 0 & \text{if } |\vec{k}| > k_0 \end{cases} \tag{8}$$

Figure 3 presents the theoretical wavenumber spectrum for an acoustical diffuse field of frequency $f_0 = 8\,000$ Hz and of amplitude $S_{pp} = 10^5$ Pa^2/Hz as expressed by equation (8), and compares it to the same spectra obtained by the post-processing of the theoretical cross-power spectra of equation (7) sampled on the array positions. Both cartographies have the same aspect, but one can observe in Figure 3-b three groups of circles, due to the aliasing provoked by the spatial sampling of the cross-power spectrum. The smaller circles have a radius of $k_{max3} \pm k_0$ with $k_{max3} = 2\pi/\Delta r_3 = 393$ rad/m, and correspond to the aliasing provoked by the most spaced transducers. The second group of circles correspond to $k_{max2} = 2\pi/\Delta r_2 = 785$ rad/m, and is provoked by the medium-sized probes. The most important effect of spatial aliasing is visible at $k_{max1} = 2\pi/\Delta r_1 = 1570$ rad/m, due to spacing between the smallest probes. Another type of aliasing can be observed and attributed to the spacing in the azimutal direction $r\sin(\Delta\theta)$. It appears by regularly spaced spots in circle shape.
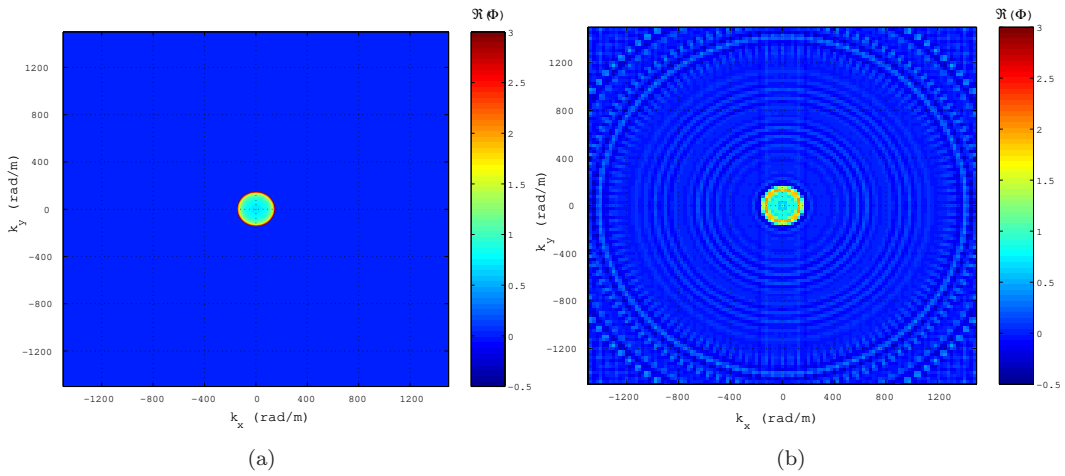
Figure 3. *Wavenumber spectrum of a diffuse sound field of amplitude 10^5 Pa^2/Hz and frequency 8 000 Hz. (a) Theoretical expression - (b) Post-processing of the theoretical cross-power spectra*
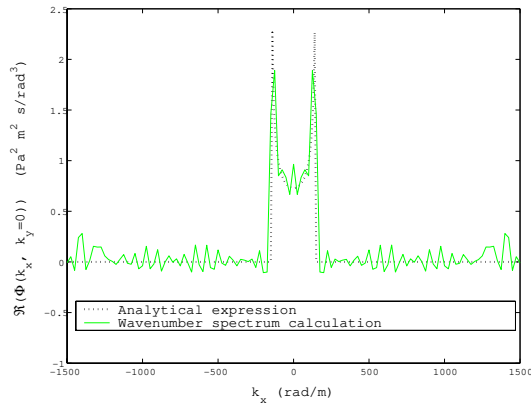

Figure 4. *Comparison of the theoretical and post-processed wavenumber spectra in one dimension for a diffuse sound field of amplitude 10^5 Pa^2/Hz and frequency 8 000 Hz.*

American Institute of Aeronautics and Astronautics

3. Corcos model

An empirical model of cross-power spectrum has been suggested by Corcos to describe pressure fluctuations on a plane wall under a turbulent boundary layer:

$$S_{p_i\,p_j}(x,y,\omega) = A(\omega)e^{-\frac{k_c}{\alpha}|x|}\,e^{-\frac{k_c}{\beta}|y|}\,e^{ik_c x}, \tag{9}$$

where $k_c = \omega/U_c$ represents the convection of vortical structures at the mean velocity U_c. The corresponding wavenumber spectrum can be calculated analytically and yields

$$\Phi(k_x, k_y, \omega) = \frac{A(\omega)}{\pi^2}\,\frac{\alpha k_c}{k_c^2 + \alpha^2(k_x - k_c)^2}\,\frac{\beta k_c}{k_c^2 + \beta^2 k_y^2}. \tag{10}$$

(a)   (b)
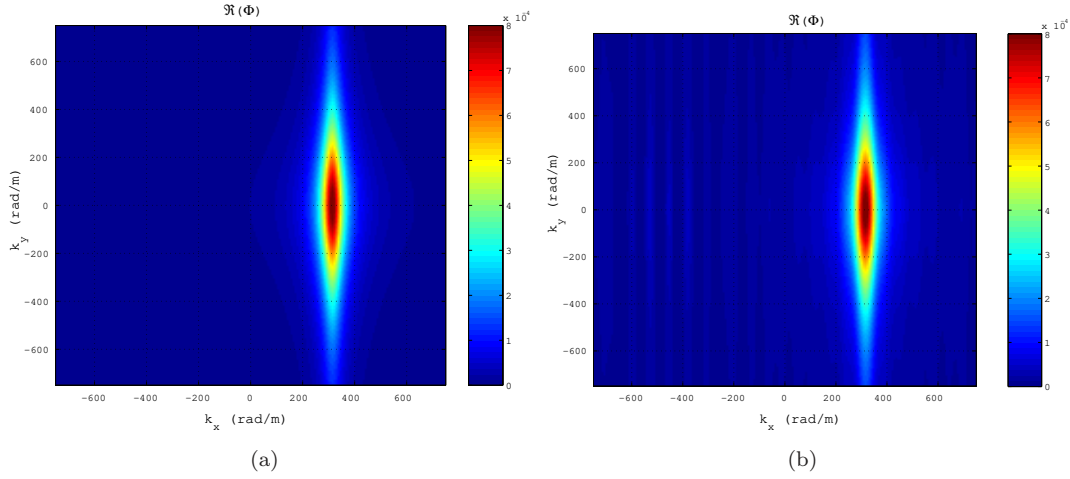
Figure 5. *Wavenumber spectrum of a Corcos pressure field ($\alpha = 8$, $\beta = 1$, U_c=40). (a) Theoretical expression - (b) Post-processing of the theoretical cross-power spectra*
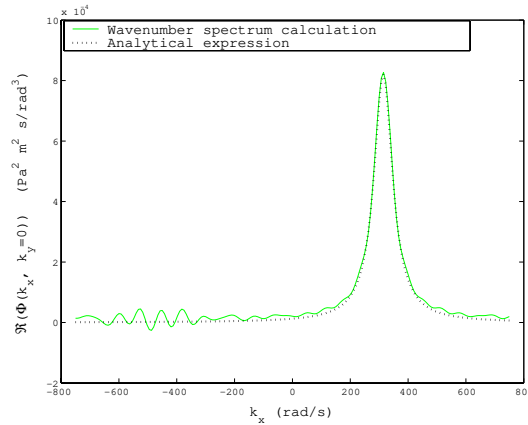
Figure 6. *Comparison of the theoretical and post-processed wavenumber spectra in one dimension for a Corcos pressure field ($\alpha = 8$, $\beta = 1$, U_c=40).*

Figures 5 and 6 allow to compare the theoretical expression (10) and the post-processing of the theoretical cross-power spectrum (9) sampled at the array points. Data for this comparison are: α=8 and β=1 corresponding to a classical boundary layer (see reference 8), $A = 100$, $U_c = 40$m/s, and the frequency is 2000 Hz, thus the convection wavenumber is $k_c = 314$ rad/m. Apart from the side lobes due to the rectangular windowing, both spectra are very similar; the peak shape in particular is well preserved. The maximum of the spectra lies at $(k_x, k_y) = (k_c, 0)$, and its width is regulated by the spatial coherence coefficients α and β.

The post-processing is validated on these two academic cases and will be now applied to measured data.

American Institute of Aeronautics and Astronautics

III. Results for a turbulent boundary layer

A. Presentation of the case

The experiments were conducted in the large anechoic wind tunnel of Ecole Centrale de Lyon[23] (France). The boundary layer studied is the one that develops naturally on the ground of the wind tunnel. Measurements were carried out at three different velocities: 30, 40, and 50m/s, but only results at 40m/s will be detailed in this paper.

The longitudinal velocity profile is presented in Figure 7 for U_∞=40 m/s. The corresponding displacement thickness is $\delta^* = 10.5$ mm.
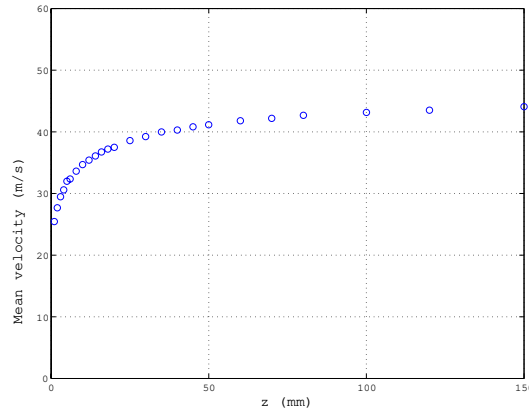
Figure 7. *Longitudinal velocity profile as a function of the distance to the ground for U_∞=40 m/s*

B. Wavenumber spectra

According to the equation (6), the wavenumber transform has been calculated on the pressure fluctuations recorded by the array. Figure 8 presents the real part of the wavenumber transform. The aerodynamic spot has the shape of a classical Corcos-like spectrum. The mean convection velocity that is deduced from this plot is 33.8 m/s. In addition, a spot is visible at low wavenumbers: this demonstrate that acoustical waves are present. The wavenumber resolution of the post-processing is not sufficient to describe the shape of the acoustic spot more precisely, but there seems to be no priviledged direction of propagation, rather a diffuse sound field.
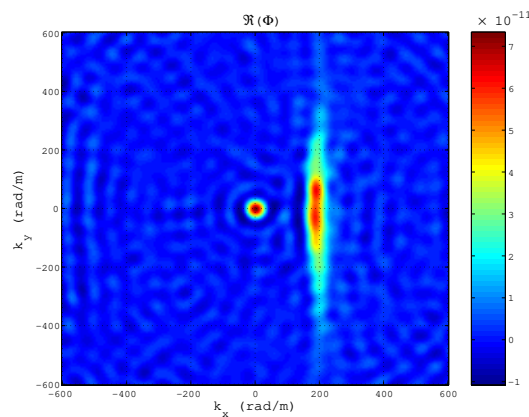

Figure 8. *Wavenumber spectrum for the boundary layer at 40 m/S and 1 000 Hz*

The rest of the paragraph will be devoted to the evaluation of the amplitude of the acoustic part and the physical explanation of its origin.

American Institute of Aeronautics and Astronautics

C.   Evaluation of the acoustic part

To evaluate the acoustic part, we first use equation (5) and integrate the wavenumber spectra over a disk of radius k_0, where $k_0 = 2\pi f/c_0$, to obtain the acoustical power spectral density.
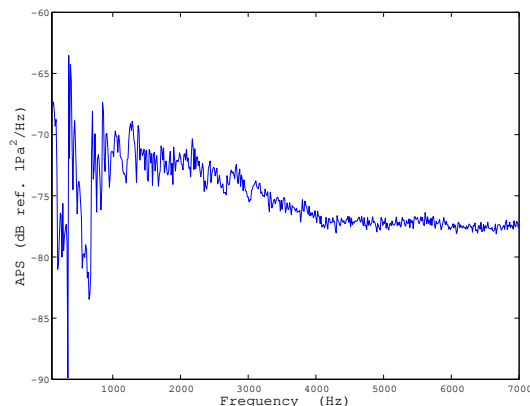

Figure 9. *Acoustical spectral density obtained by integration of the wavenumber spectrum*

Figure 9 shows the evolution of the amplitude of the acoustical auto-power spectra with frequency. Two peaks at 345 Hz and 690 Hz are clearly visible on the graph. They are suspected to come from the modal resonances of the square-section duct. If we consider the wooden duct as rigid, its resonance frequencies are $f_n = nc_0/2L$ with length $L = 50$ cm, that is to say $f_n = 343n$ Hz, which corresponds to the measured peaks. To ensure this interpretation, a new measurement has been conducted by submitting the duct to a white noise and measuring the resulting pressure on the probes. Figure 10 presents the transfer function between the sound source and the microphone probes placed along the longitudinal direction. At low frequency one can clearly distinguish the first modes of the duct at 340 and 680 Hz, corresponding to the theoretical resonance frequencies for a rigid duct (red dotted lines). The other frequency peaks can be associated to the structural resonance modes of the wooden and lucite panels.
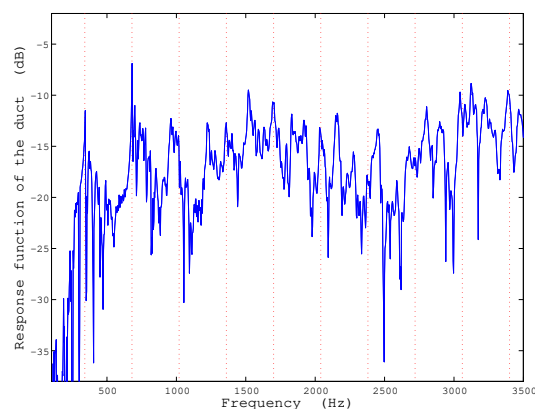

Figure 10. *Acoustical response of the duct when excited with a white noise. Red dotted lines stand for theoretical resonance frequencies for a rigid duct.*

A second method to evaluate the acoustic part is to study the cross-power spectra. Figure 11 shows the coherence γ as a function of the distance to the center. According to Corcos model, it should be of exponential form, that is why we plotted $\ln(\gamma)$. Here the graph is not linear but shows regular oscillations. A linear interpolation on the central points of this graph would then lead to wrong values of the parameters. These oscillations are produced because of the existence of acoustic waves generated by the boundary layer. Based on the observation of Figure 8, we suppose that the pressure field has the theoretical form of a Corcos
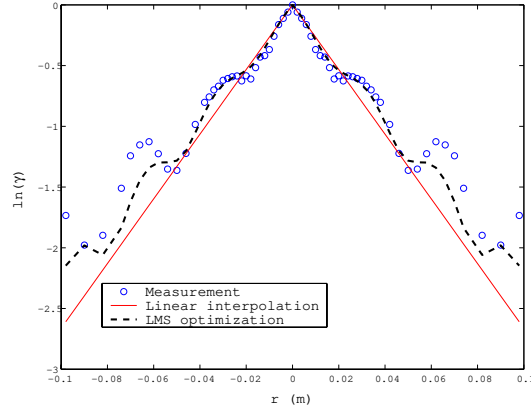
American Institute of Aeronautics and Astronautics

Figure 11. *Coherence function of pressure signals in the longitudinal direction at 1 000 Hz*

pressure field perturbed by a diffuse acoustic field:

$$\frac{S_{pp}(r,\theta,\omega)}{S_{pp}(0,0,\omega)} = e^{-\frac{\omega}{\alpha U_c}|r\cos\theta|}\, e^{-\frac{\omega}{\beta U_c}|r\sin\theta|}\, e^{i\frac{\omega}{U_c}r\cos\theta} + A\operatorname{sinc}(k_0 r). \qquad (11)$$

We then try to find by least mean square minimization the Corcos coefficients α, β, U_c and the acoustic magnitude A to fit the experimental data. Ibars[5] already performed such an optimization on its data, but with a plane wave model for the acoustic component. For time-saving reasons, we do not use the whole 3 969 measurement points, but all the 63 probes for only 11 regularly distributed angular position of the disk. Results are presented in Figures 12 to 16.
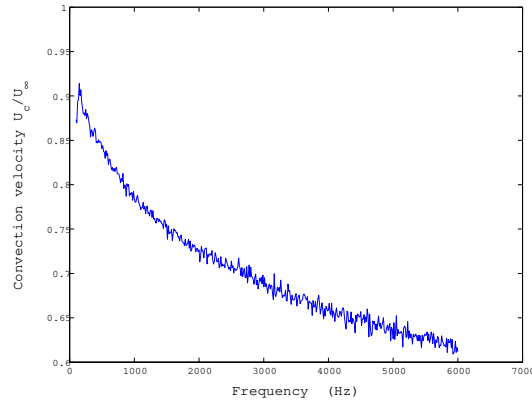

Figure 12. *Evolution of the Corcos convection velocity U_c with frequency, resulting from the LMS optimization*

One can immediately note that none of the Corcos coefficients is constant with frequency. Decrease of the convection velocity while frequency increases has already been observed,[8] and is often interpreted in term of size of structures. As frequency increases, the size of structures in the boundary layer, proportional to the wavelength, decreases. Small vortex are thus located nearer to the wall than large structures, and are submitted to a slower flow. Their convection velocity is therefore smaller.

Figure 13 shows the evolution of the correlation coefficients α and β: decrease with frequency for α and increase for β. For more physical interpretation, we represent the longitudinal correlation length $\alpha U_c/\omega$ and the transversal correlation length $\beta U_c/\omega$ as functions of the frequency (Figure 14). The obtained curves are not straight. This means that, on the contrary of Corcos assumption, correlation lengths do not evolve as the inverse of frequency. One can notice that the correlations in both directions evolve similarly at high frequency.

In what concerns the acoustic magnitude, it is represented in Figure 15 in percentage of the aerodynamic magnitude. On the main part of the frequency band, the acoutical magnitude represents about 5% of the
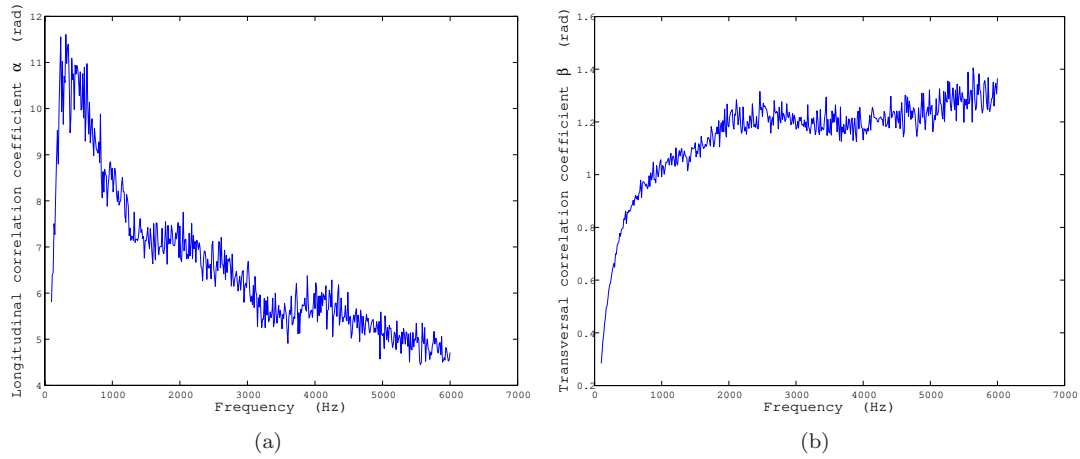
American Institute of Aeronautics and Astronautics

(a)

(b)

Figure 13. *Evolution of Corcos coefficients with frequency, resulting from the LMS optimization (a) α coefficient - (b) β coefficient*
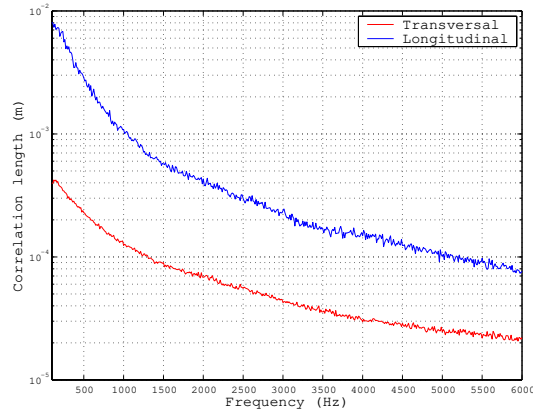

Figure 14. *Evolution of longitudinal and transversal correlation lengths with frequency, resulting from the LMS optimization*
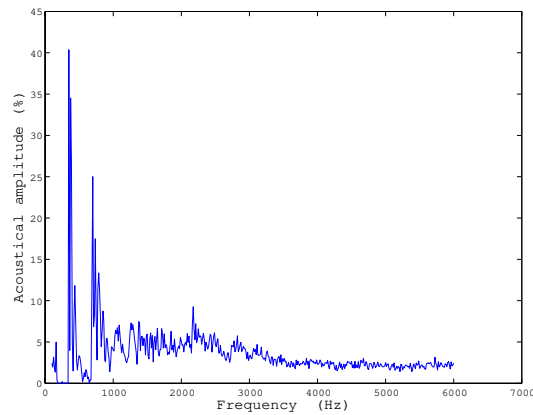

Figure 15. *Evolution of the diffuse acoustic pressure magnitude with frequency, resulting from the LMS optimization*
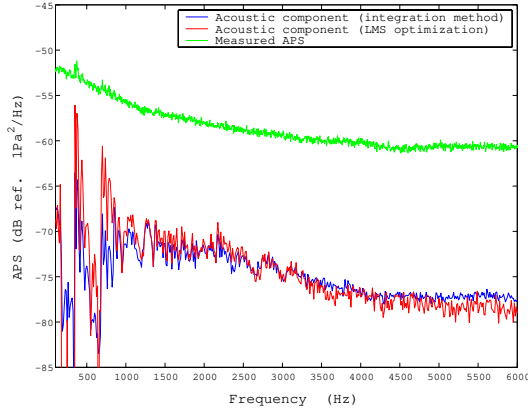
American Institute of Aeronautics and Astronautics

Figure 16. *Comparison of the acoustical amplitude obtained by integration of the wavenumber spectrum and by least mean square optimization on CPS*

aerodynamic magnitude. There is thus a difference of 13 dB between the acoustic component and the aerodynamic component of the wall pressure fluctuations, which is much fewer than the difference of 25 dB found in the simulations of Dejong et al.[3] At resonance frequencies of the duct, the acoustical magnitude reaches nearly 45% of the aerodynamical magnitude, what shows the power of resonance phenomena. For better comparison with the first calculation method, the acoustical magnitude has been multiplied by the APS level to obtain the real acoustical magnitude in Pa^2/Hz. Figure 16 shows that both methods are in very good agreement. The second resonance peak is not well marked for the integration method, probably because of a lack of precision of this method due to the crude spectral sampling ($\Delta k = 6$ rad/s to compare with $k_0 = 12.6$ rad/s for this frequency). This implies that the round shape of the acoustic spot is not well described at low wavenumber.

Directivity of the produced acoustic waves is now discussed. To this end, the maximum in the acoustical spot has been looked for in each wavenumber spectrum, and his position has been recorded. Figure 17 shows the distribution of those maxima as a function of frequency. Whereas the k_y values seem to be evenly distributed between $-k_0$ and k_0, this is not the case for the longitudinal wavenumber. Though the effect of discretization is visible, it is clear that k_x values are always positive. These observations shows that acoustic waves propagates have a prefered propagation direction, namely the downstream direction. Two hypothesis can then be formulated about the origin of these waves.

- The acoustical waves come from the flow generation system, which is located upstream the measurement area. However, in this case, the exhaust jet noise that propagates upstream would also have been detected. This noise has indeed the highest level in the facility.

- The acoustical waves are produced by the local structures in the boundary layer and are evenly distributed in the flow; however they do not have a diffuse radiation but an intrinsic directivity. The origin of such a directivity is still unclear but could come from diffraction of acoustic waves by velocity gradient of the boundary layer.

IV. Results for a cylinder in the flow

A. Presentation of the case

The second case studied is the one of a cylinder placed 18 cm upstream the measurement central point. For practical reasons, the diameter of the bar is not constant, as visible in Figure 18. The upper part has a diameter of $D_1 = 1.7$ cm whereas the lower part has a diameter of $D_2 = 2.1$ cm. The corresponding Reynolds numbers are $Re_{D_1} = 45300$ and $Re_{D_2} = 56000$. According to theory,[21] a wake forms downstream of the cylinder, which contains the most energetic structures. At a particular frequency determined by a fixed Strouhal number
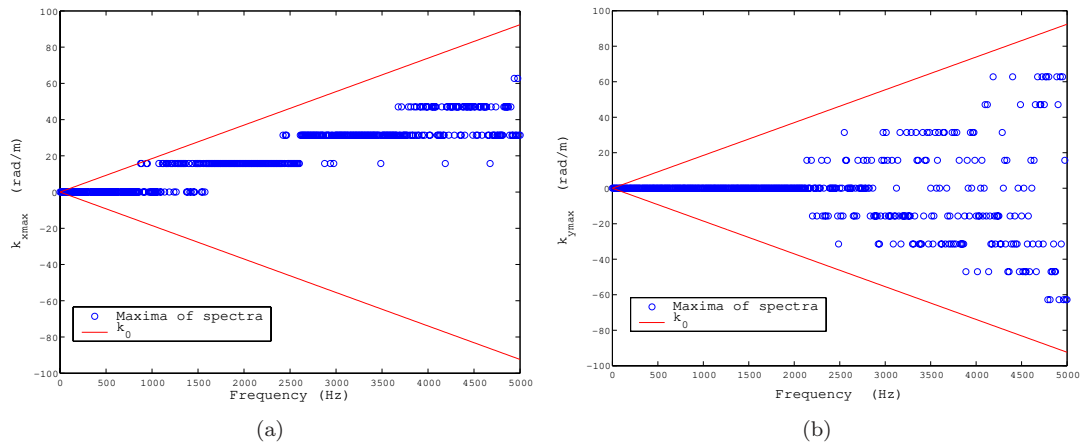
$$St = \frac{fD}{U_\infty},$$

American Institute of Aeronautics and Astronautics

Figure 17. *(a) Longitudinal and (b) transversal wavenumber corresponding to maximum of the acoustical spot as a function of frequency*

Figure 18. *Photograph of the duct equipped with the bar upstream the rotating measurement disk*

a periodic phenomenon appears : vortex are shedded peridically in the wake, forming the Von Kármán street.

A far field measurement has been performed by placing a microphone 1 m beside the duct exhaust. Figure 19 shows that there are two whistling frequencies at $f_1 = 381$ Hz and $f_2 = 509$ Hz. These frequencies correspond to Strouhal numbers of

$$St_1 = 0.200 \text{ for } D_1 = 2.1 \text{ cm,}$$

$$St_2 = 0.216 \text{ for } D_2 = 1.7 \text{ cm,}$$

which are near the value of 0.21 found in the classical litterature.[21] Another peak is visible in this figure at about 343 Hz, as previously observed for the boundary layer case, which has been identified as the first mode of the duct. In this figure, the peaks are not very sharp and well defined. This is probably due to an interaction process between the shedding phenomena. Still the main peaks are easily visible.
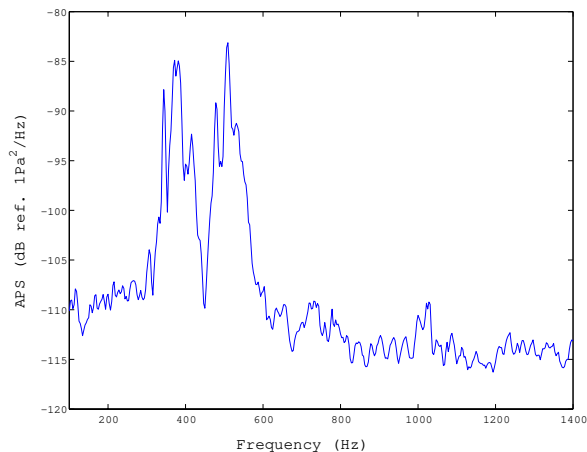

Figure 19. *Far-field measurement of the pressure emitted by the bar*

On the measurement probes, the location of the Strouhal peaks is variable, as shown in Figure 20: probes located near the axis of the bar do not exhibit the peaks, whereas probes situated rather far from this axis exhibit strong peaks. Probes located between the two present a bump at the first whistling frequency. This should be linked to the dipolar directivity of a whistling bar. In the bar-flow axis, namely in the longitudinal direction, the acoustical radiation of the bar is very small. The pressure observed is then essentially of aerodynamic origin. By going far away from the bar axis, the level of aerodynamic pressure decreases since the probes are out of the wake. Moreover, since the measurement area is rather far downstream of the bar, the wake is unstructured producing a bump and not a peak at the whistling frequencies. By going farther away from the bar axis, the probes are not submitted to the bar wake anymore, and except at whistling frequencies, their pressure level is similar to the one of the boundary layer at the same velocity. According to the directivity of a dipole, the acoustical level far from the bar axis increases. The level of the acoustical peaks is thus more visible on probes located far away from the axis.

Theoretically, spatial homogeneity is needed to calculate wavenumber spectra. Preliminary observations show that this is not the case. In order to obtain quantitative data about this inhomogeneity, Figure 21 plots the ratio of pressure level measured by every transducer to the one measured by the central probe. The left figure shows the wake of the cylinder of strong energy, and, around it, a region of lower energy. This pattern widens by going downstream, showing the wake's natural expansion. At the whistling frequency (Figure 21-b), the pattern is modified. Points situed transversally to the flow exhibit a greater spectral density than those located near the longitudinal line, which corresponds to the phenomenon of dipolar acoustic radiation observed in Figure 20.

B. Wavenumber spectra

Wavenumber spectra were then calculated on the basis of equation (6). Figure 22-a shows the wavenumber spectra for a frequency of 381 Hz, corresponding to the first whistling.
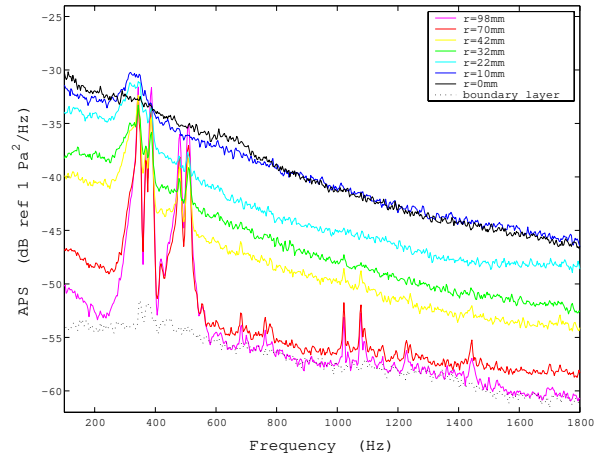
American Institute of Aeronautics and Astronautics

Figure 20. *Some APS of probes placed transversally to the flow*

(a)   (b)
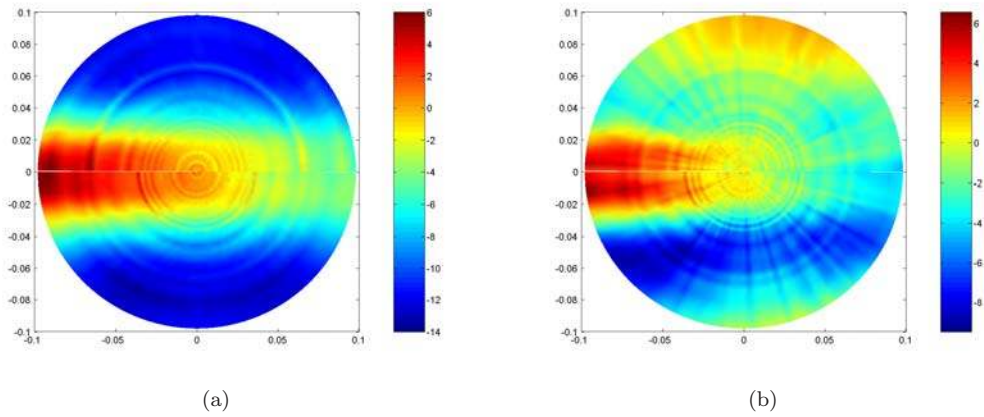
Figure 21. *(a) Ratio of filtered RMS level measured by each microphone probe to the central probe filtered RMS level. Filtered RMS values are obtained by integrating the APS over the frequency band [100 Hz-6 000 Hz] - (b) Ratio of APS level measured by each microphone probe to the central probe APS level at 381 Hz (whistling frequency)*
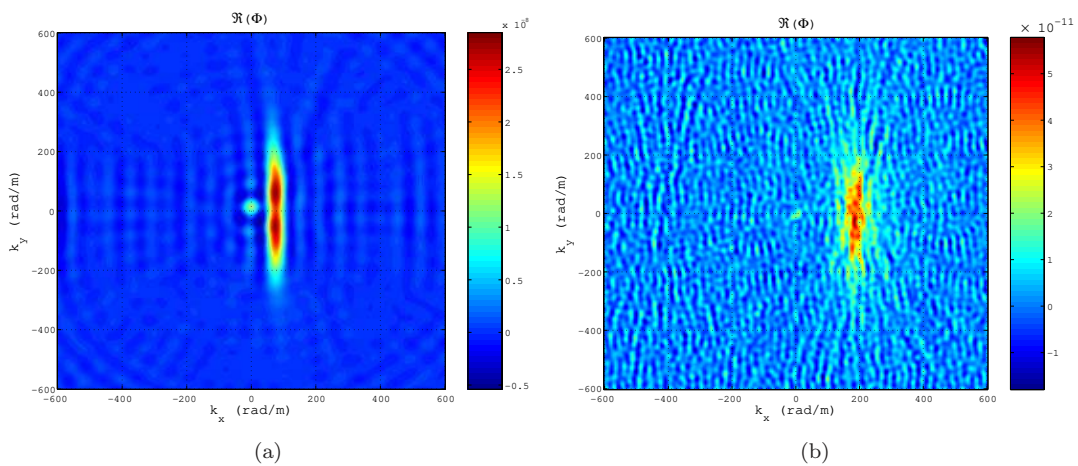

(a)   (b)

Figure 22. *Wavenumber frequency spectrum for the bar case at U_∞ =40 m/s (a) f=381Hz - (b) f=600 Hz*

American Institute of Aeronautics and Astronautics

At low wavenumbers, an acoustical phenomenon can be observed, whereas a Corcos-like aerodynamic spot is present at upper wavenumbers. The wavenumber resolution brought by the array does not allow us to examine the shape of the acoustic spot further, but it does not seem to present a privileged direction of propagation. On the contrary, the aerodynamic spot presents two maxima, corresponding to the main propagation directions of the Von Kármán vortexes.

To compare, a wavenumber spectrum is presented at 600 Hz, where the bar is not whistling. The acoustical spot is not present in this figure. The quality of the wavenumber spectra has however much deteriored.

For comparison with the boundary layer wavenumber spectrum of Figure 8, the wavenumber spectrum at 1 000 HZ for the bar is shown in Figure 23. As observed at 600 Hz, the spectrum is very noisy, but the aerodynamic spot is still visible. The imaginary part of Φ is of the same order of magnitude than the real part, revealing that the pressure pattern is not symetric about the central point.

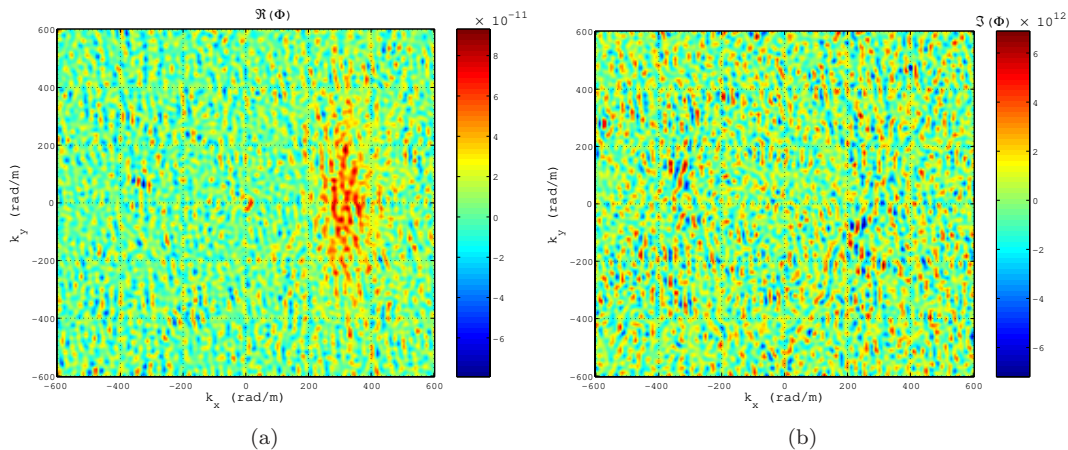(a)   (b)

Figure 23. *(a) Real and (b) imaginary part of the wavenumber frequency spectrum for the bar case at $U_\infty=40$ m/s and $f=1000Hz$*

Explanations for these noisy spectra are now sought. To this end, Figures 24 and 25 plot the coherence values at 1 000 Hz for two angular positions of the probes line (0 and 29°), and the corresponding phases. Curves are as smooth as for the boundary layer case. As a conclusion, noise on the wavenumber spectra does not come from noisy measurements. Corcos-like coefficients were calculated by linear interpolation on the first central points and are similar to the boundary layer case: $\alpha=7.5$, $\beta=0.76$ and $U_c = 0.79U_\infty$.

Besides, it can be noticed that the previously observed oscillations are present on the oblique coherence, revealing the presence of acoustical waves. These acoustic waves do not correspond to any duct resonance or bar whistling, but to broadband acoustics. Those oscillations are not visible on the longitudinal coherence. Indeed, in the longitudinal direction, the probes are located in the cylinder wake, which is the most energetic region of the flow. For a given wavelength, the aerodynamic level is then much higher than the acoustic one. That is why the acoustical waves are not observed in the longitudinal direction.

It was then shown that the noise on wavenumber spectra does not come from the data, neither from the post-processing. In fact, the problem comes from the inhomogeneity of the flow: theoretically, it is not possible to calculate a wavenumber spectra in the bar, since equation (4) is only valid for homogeneous pressure fields.

V.   Conclusion

Direct measurements of the wavenumber-frequency spectrum of pressure fluctuations under turbulent flows using an original rotative array of 63 remote microphone probes were performed.

Results obtained for the boundary layer are consistent with the classical models. Moreover, it was pointed out the existence of a broadband acoustical component, which level represents 5% of the aerodynamic amplitude.

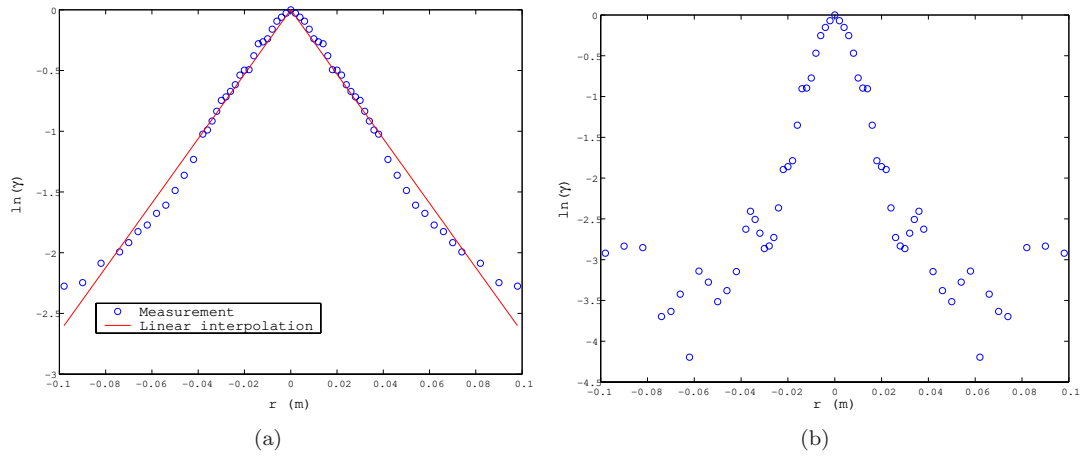The case of the cylinder in cross-flow was found to be highly inhomogeneous: probes in the bar wake

American Institute of Aeronautics and Astronautics

Figure 24. *Coherence function of pressure signals at 1 000 Hz (a) at 0° - (b) at 30°*
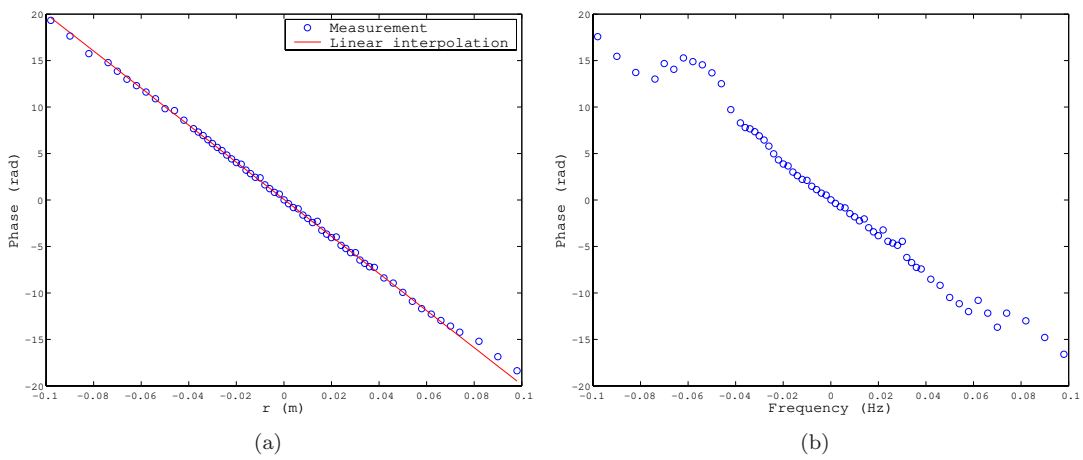
Figure 25. *Phase of pressure signals at 1 000 Hz(a) at 0° - (b) at 30°*

American Institute of Aeronautics and Astronautics

do not exhibit acoustical pressure components, whereas peaks are visible on autospectra of probes located outside the wake. The characteristic dipolar directivity of a whistling bar was observed. Whistling frequencies measured in the far field were also found on wavenumber spectra. Besides, this case shows the limits of the wavenumber post-processing for inhomogeneous flows.

Comparison of the acoustic field in both cases allows to conclude that broadband acoustics can only be detected if the aerodynamic level in the low wavenumber region is not too high compared to the acoustical one. In order to obtain the acoustic level, the measurement has to be performed in a rest fluid region. The measurement set-up and the post-processing are finally validated and will be used for more realistic configurations including separated and reattached flows.

Acknowledgments

References

[1] A.R.George 1990 "Automobile aerodynamic noise" SAE Paper 900315

[2] P.G.Bremner & J.F.Wilby 2002 "Aero-vibro-acoustics : problem statement and methods for simulation-based design solution" AIAA Paper 2002-2551

[3] R.G.DeJong, T.S.Bharj & J.J.Lee 2001 "Vehicle wind noise analysis using a SEA model with measured source levels" SAE Paper 2001-01-1629

[4] W.K.Bull 1996 "Wall-pressure fluctuations beneath turbulent boundary layers : some reflections on forty years of research" Journal of Sound and vibration, No.190, Vol.3, pp.299-315

[5] P.Ibars 1990 "Contribution des petits nombres d'onde au champ pariétal de pression dans une couche limite turbulente bidimensionnelle. Comparaison de différentes techniques expérimentales" Thèse de doctorat, Ecole Centrale de Lyon, No. 90-15

[6] E.Manoha 1993 "Mesure du spectre en fréquences et nombres d'ondes du champ des fluctuations de pression pariétale sous une couche limite turbulente" Thèse Université Paris VI, No. 93PA06673

[7] B.M.Abraham & W.L.Keith 1998 "Direct measurements of turbulent boundary layer wall pressure wavenumber-frequency spectra" Journal of Fluid Engineering, Vol.120, pp.29-39

[8] W.E.Blake 1986 "Mechanics of flow-induced sound and vibration" Academic Press, Orlando, Florida, Applied Mathematics and Mechanics, Vol.II : Complex flow-structure interaction

[9] G.Robert 1984 "Modélisation et simulation du champ excitateur induit sur une structure par une couche limite turbulente" Thèse de doctorat, Ecole Centrale de Lyon, No. 84-02

[10] G.Maidanik 1967 "Flush-mounted pressure transducer systems as spatial and spectral filters" Journal of the Acoustical Society of America, Vol.42, No.5, pp.1017-1024

[11] G.Maidanik & D.W.Jorgensen 1964 "Boundary wave-vector filters for the study of the pressure field in a turbulent boundary layer" Journal of the Acoustical Society of America, Vol.42, No.2, pp.494-501

[12] P.Bally, P.Olivero, P.Hocquet & B.E.Forestier 1990 "Spectre nombre d'onde-fréquence des fluctuations de pression sous couche limite turbulente en gradient de pression nul et positif" Journal d'Acoustique, Vol.3, pp.125-136

[13] W.K.Blake & D.M.Chase 1971 "Wavenumber-frequency spectra of turbulent boundary-layer pressure measured by microphone arrays" Journal of the Acoustical Society of America, Vol.49, No.3, Part 2, pp.862-877

[14] G.M.Corcos 1963 "Resolution of pressure in turbulence" Journal of the Acoustical Society of America, Vol.35, No.2, pp.192-199

[15] C.H.Sherman, S.H.Ko & B.G.Buehler 1990 "Measurement of the turbulent boundary layer wave-vector spectrum" Journal of the Acoustical Society of America, Vol.88, No.1, pp.386-390

[16] R.M.Lueptow 1995 "Transducer resolution and the turbulent wall pressure spectrum" Journal of the Acoustical Society of America, Vol.97, No.1, pp.370-378

[17] J.R.Callister 1996 "Measurement, prediction, and reduction of the transmission of separated flow noise through panels" Ph. Dissertation, Faculty of the Graduate School of Cornell University, UMI number 9639625

[18] T.M.Farabee & M.J.Casarella 1986 "Measurement of fluctuating wall pressure for separated/reattached boundary layer flows" Journal of Vibration, Acoustics, Stress and Reliability in Design, Vol.108, pp.301-307

[19] T.M.Farabee & M.J.Casarella 1991 "Spectral features of wall pressure fluctuations beneath turbulent boundary layers" Phys. Fluids A, Vol.3, No.10, pp.2410-2420

[20] T.A.Brungart, G.C.Lauchle, S.Deutschland & E.T.Riggs 2002 "Wall pressure fluctuations induced by separated/reattached channel flow" Journal of Sound and Vibration, Vol.251, No.3, pp.558-577

[21] W.E.Blake 1986 "Mechanics of flow-induced sound and vibration" Academic Press, Orlando, Florida, Applied Mathematics and Mechanics, Vol. I : General concepts and elementary sources

[22] A.D.Pierce 1991 "Acoutics. An introduction to its physical principles and applications" Acoustical Society of America, second printing

[23] M.Sunyach, B.Brunel, G.Comte-Bellot 1985 "Performances de la soufflerie anéchoique à grandes vitesses de l'école centrale de Lyon" Revue d'Acoustique, No.73